Fermilab

FN-328
1111.140

ENERGY DEPOSITION IN TARGETS AND BEAM DUMPS AT 0.1-5 TeV PROTON ENERGY

N.V.Mokhov*

Institute for High Energy Physics

Serpukhov, USSR

August 8, 1980

ABSTRACT

Modifications of the Monte Carlo program MARS and comparisons with other programs are described. Regularities of energy deposition formation in targets and beam dumps irradiated by 0.1-5 TeV protons are investigated. Enthalpy reserves and admissible energy deposition densities are calculated for some materials. Tolerable beam sizes in the 10^{12} to 10^{15} intensity range are determined.

*Visiting Scientist at Fermilab, December 1979 to September 1980

I. INTRODUCTION

The complex accelerator projects of the generation to come, Tevatron, UNK and Pentevac for example, assume extremely high values of proton energy (up to 5 TeV) and beam intensity (up to 6×10^{14} ppp). The behavior of matter struck by such beams results in a number of macroscopic features; e.g., instantaneous melting, explosion, cracking and long-term effects. The cause of these features, energy deposition during hadronic and electromagnetic shower development, is the subject of this paper. Throughout the paper we assume beam spill times which are short compared to the conduction time constant of the struck material.

II. MARS-7 AND MARS-8 PROGRAMS

The three-dimensional nuclear-electromagnetic cascades are calculated exclusively with Monte Carlo programs. The present study is performed with the MARS computing complex[1-3] which uses phenomenological formulas for inclusive hadron production in the energy region from a few MeV up to a few TeV. Other features of the MARS programs are absorption cross section energy dependence, an exact description of hadron-proton interactions, the possibility for point-like detectors, and the analytical geometry methods used for particle transport and three-dimensional geometry description.

MARS-4[3] is the basic program. MARS-5[4] was designed for calculations of p, n, π^+, π^-, k^+, k^-, $\bar{p}$ distributions from a target as well as the stopping densities of negative hadrons (π^-, k^-, $\bar{p}$, Σ^-). MARS-6[5] makes it possible to consider in a convenient way the effect of magnetic and electric fields and also the azimuthal

structure of the constructions. Note also the special ultra-relativistic version for DUMAND acoustic studies.[6]

In general the results of the calculations agree well with experimental data as well as with CASIM[7,8] predictions.[3,9] However recent study[9] has shown the great importance of precision in the description of the energy deposition from low energy hadrons and electromagnetic showers from π^0 decays. The program MAXIM was created[10] which is the combination of CASIM[7] and the electron-photon shower program AEGIS,[8] and which also considers the transport of low energy protons.[9]

Similar features were introduced in the MARS programs. The main modifications in creating MARS-7 and MARS-8 programs are:

1. A new description of electromagnetic showers from neutral pion decays, radial dependent empirical formula from Ref. 7 in MARS-7 and quasianalog simulation of electron-photon showers from Ref. 8 in MARS-8.
2. The transport of evaporated protons and neutrons, nucleons from π^- capture and subthreshold nucleons; it gives in some cases a factor of two because the range of such particles can exceed the small beam and radial bin sizes.
3. A better description of Coulomb and elastic scatterings for initial hadrons.
4. A slight improvement in the energy dependence of absorption cross sections at the highest energies.

III. RESULTS: COMPARISONS AND REGULARITIES

In this section we present the results of the calculations of energy deposition density distributions, $\mathcal{E}$, in the central parts of targets and beam dumps irradiated by 0.1-5 TeV proton beams of various sizes. Graphite with density $\rho = 1.71$ g/cm^3 has been chosen as the most appropriate (from melting and cracking points of view) material for such applications. In one case BeO ceramic has been considered.

The beam distribution is Gaussian in both vertical and horizontal profiles with standard derivations of σ_v and σ_h, respectively. In all cases the smallest radial bin has been chosen as $0 \le r \le 0.5\sigma\text{min}$, which is related to the real maximum energy deposition density $\mathcal{E}_{max}$.[9]

The longitudinal distributions of energy deposition density $\mathcal{E}$ at various radial intervals are shown in Figs. 1-4 for 100, 400, 1000, and 3000 GeV proton energies. These figures show the results of MARS-7, MARS-8, CASIM, and MAXIM calculations (the last two only at $E_0 \le 1000$ GeV where they work). It is remarkable that the data of pairs (MARS-7, CASIM) and (MARS-8,MAXIM) agree very well in spite of very different physical and calculative schemes used. The factor of 1.5-2 disagreement at the shower maximum inside pairs (MARS-7, MARS-8) and (CASIM, MAXIM) arises evidently from the different description of the electromagnetic shower.

Three conclusions result from these comparisons:

1. Since four different programs agree with each other to the extent seen in Figs. 1-4, we feel reassured that the absolute value of the energy deposition is believable within a factor of 1.5-2.
2. We recommend the use of MAXIM (at $E_0 \leq 1$ TeV) and MARS-8 because they incorporate the most accurate description of the electromagnetic shower.
3. A cheaper approximation (factor of two on the average) is achieved by running of CASIM or MARS-7 (compared with MAXIM or MARS-8).

The rest of the results presented in this paper have been obtained with the MARS-8 program.

The spatial distributions of energy density for a large 3 TeV proton beam are shown in Fig. 5. Figure 6 is a collection of longitudinal maximum energy density distributions for incident protons in the 0.1 to 5 TeV energy range. It is interesting to note a transformation of curves with energy.

Figure 7 shows the radial dependence of $\mathcal{E}/E_0$ values at shower maxima for E_0 = 0.4, 1, 3, and 5 TeV for two various beam sizes. There is no radial dependence at $r<0.5\sigma$ min. At $E_0 \geq 1$ TeV and r>1 cm energy deposition divided by E_0 does not depend on initial energy (scaling). In this region the radial dependence can be approximated by the expression

$$\frac{\mathcal{E}}{E_0} = 4.1\times10^{-5}\ r^{-2.32},\ \frac{1}{g\times 1\ \text{inc-proton}} \qquad (1)$$

where $1<r<10$ cm, $\sigma<1$ cm, $E_0 \geq 1000$ GeV, $[\mathcal{E}] = \text{GeV}\times g^{-1}\times 1$ inc-proton^{-1}. For other conditions the slope in Eq. (1) will be slightly changed.

The energy dependences of maximum energy deposition densities $\mathcal{E}_{max}$ are presented in Fig. 8 for various beam sizes. It is remarkable that we can describe these dependences in wide region with simple law

$$\mathcal{E}_{max} = A\times E_0^n, \ \text{GeV}\times g^{-1}\times 1 \text{ inc-proton}^{-1}, \qquad (2)$$

where E_0 in GeV and parameters A and n for graphite target are listed in the table below:

Beam	σ_v, cm	σ_h, cm	E_0, GeV	$A\times 10^5$	n
1	0.07	0.14	400-3000	2.3	1.44
2	0.7	1.4	100-5000	1.3	1.20
3	2	4	100-5000	.48	1.13

Figure 9, which also uses data from a previous paper[9], shows the $\mathcal{E}_{max}$ dependence on beam area defined as

$$B = 4\pi\ \sigma_v\ \sigma_h. \qquad (3)$$

Data are presented for 0.1, 0.4, 1, 3, and 5 TeV. 1 TeV results are shown for three different beam shapes $\sigma_h = \sigma_v$, $\sigma_h = 2\sigma_v$, $\sigma_h = 10\sigma_v$. As was first noted in Ref. 9, results are completely independent of beam shape. At the smallest areas and $E_0 \leq 1$ TeV the data are independent of initial energy.

IV. TEMPERATURE RISE AND LIMITS

The instantaneous temperature rise in the considered bulk of matter can be determined from the calculated energy deposition

distributions and from an enthalpy reserve. The latter is determined as

$$\Delta H(T) = \int_{T_0}^{T} C_p\,(T^1)\,dT^1, \qquad (4)$$

where T_0 and T are the initial and final temperatures, respectively, and $C_p(T)$ is the heat capacity.

Using thermophysical data from Ref. 11, we have calculated Eq. (4) and results for graphite and BeO are presented in Fig. 10. At T_0 = 20°C and T≥100°C Eq. (4) for graphite gives

$$\Delta H(T) = 0.165 \times T^{1.31}, \ \frac{\text{Joules}}{\text{g}}. \qquad (5)$$

The enthalpy reserve and the energy deposition are related by the equation

$$\Delta H(T) = 1.6\times10^{-10}\times I\times\mathcal{E}, \qquad (6)$$

where I is the number of incoming protons per pulse.

Now we can easily estimate the instantaneous temperature due to a single pulse. Solving Eqs. (5) and (6) for temperature, we obtain:

$$T = \left(\frac{1.6\times10^{-10}\times I\mathcal{E}}{0.165}\right)^{0.76336}, \qquad (7)$$

for T≥100°C.

The next relation must be valid for all parts of the considered systems

$$\Delta H\,(T_{max}) \geq 1.6\times10^{-10}\times I\times\mathcal{E}_{max}, \qquad (8)$$

where the maximum energy deposition can be determined by Eq. (2) and T_{max} is the "melting" or "cracking" temperature, whichever is smaller.

In particular for graphite H-489 we have[12]

$T_{melt} = 3500°C$

$T_{crack} = (2235\text{-}2314)°C.$

We have chosen $T_{max} \simeq 2300°C$ and from Fig. 10 or Eq. (5) we have obtained

$$\Delta H\ (T_{max}) \simeq 4000 \text{ Joules/g}.$$

The admissible energy deposition density must be

$$\mathcal{E}_{max} \leq \frac{2.5\times10^{13}}{I}, \quad \frac{GeV}{g\times 1 \text{ inc-proton}} \tag{9}$$

For any proton beams and graphite targets or beam dumps, the next fundamental limit follows from Eqs. (2) and (9)

$$E_0^n \times I \leq \frac{2.5\times10^{13}}{A} \tag{10}$$

where parameters n and A are determined in the previous table.

Now we can get tolerable beam sizes from Fig. 9 and the limitations of this section. Because the maximum energy deposition is independent of beam shape it is very convenient to consider limitations on beam area $B = 4\pi\ \sigma_v\ \sigma_h$ or particularly on $\sqrt{B}$. The minimum possible value of $\sqrt{B}$ as a function of the number of incident protons are presented in Fig. 11 for 0.1, 0.4, 1, 3, and 5 TeV protons. In the specific case $\sigma_h = 2\sigma_v$ the value of $\sqrt{B} \simeq 5\sigma_v$. Note once more that the data of Fig. 11 have been calculated for maximum instantaneous temperature in graphite $T_{max} = 2300°C$. Figure 11 has the parameters of all accelerators of new generation.

Acknowledgements:

Valuable discussions with H.Edwards, T.Murphy, T.Toohig,

F.Turkot, and A.VanGinneken are greatly appreciated. I am especially thankful to T.Murphy for his reading the text and making a lot of suggestions and to A.VanGinneken for introducing me to his programs and for many days of joint work.

References:

[1]N.V.Mokhov, in Proc. IV All-Union Conference on Charged Particle Accelerators, Moscow, 1974, V.2, M., "Nauka", 1975, p.222.

[2]N.V.Mokhov, preprint IHEP76-64, Serpukhov, 1976.

[3]I.S.Baishev, S.L.Kuchinin, N.V.Mokhov, preprint IHEP78-2, Serpukhov, 1978.

[4]A.S.Denisov, et al., preprint LINP-459, Leningrad, 1978.

[5]M.A.Maslov, N.V.Mokhov, preprint IHEP79-135, Serpukhov, 1979. To be published in "Particle Accelerators", 1980.

[6]G.A.Askarian, B.A.Dolgoshein, A.N.Kalinovsky, N.V.Mokhov, Nucl Instr.Meth. 164, 267, 1979.

[7]A.VanGinneken, Fermilab FN-272, 1975.

[8]A.VanGinneken, Fermilab FN-309, 1978.

[9]N.V.Mokhov, A.VanGinneken, Fermilab TM-977, 1980. Also in Proc. of the Workshop on High Intensity Targeting, Fermilab, April 1980.

[10]A.VanGinneken, private communication. See also H.Edwards, S.Mori and A.VanGinneken, Fermilab UPC-30, 1978.

[11]Y.S.Touloukian, Thermophysical Properties of Matter, Vol. 1, Plenum, New York-Washington, 1970.

[12]F.Turkot, T.Murphy, letter to H.Edwards, July 2, 1980, Fermilab.

Captions:

Figure 1 Energy deposition density as a function of depth Z in a graphite target (density = 1.71 g/cm^{-3}) for 100 GeV incident protons and for the radial regions indicated. The beam distribution is Gaussian in both vertical and horizontal profile with standard deviations of σ_v = 0.07 cm and σ_h = 0.14 cm, respectively. In Figs. 1-4: o - MARS-8, • - MAXIM, Δ - MARS-7, ▲ - CASIM results.

Figure 2 The same as in the previous figure but for E_0 = 400 GeV, BeO target (density = 2.85 g/cm^{-3}) and $\sigma_v = \sigma_h$ = 0.05 cm.

Figure 3 The same as in Fig. 1 but for E_0 = 1000 GeV.

Figure 4. The same as in Fig. 1 but for E_0 = 3000 GeV. Only MARS calculation results.

Figure 5 Energy deposition density spatial distribution in graphite for 3000 GeV incident protons. σ_v = 2 cm and σ_h = 4 cm. MARS-8 results are presented here and in the next figures.

Figure 6 Longitudinal distributions of maximum energy deposition in graphite for various incident energies. σ_v = 0.07 cm and σ_h = 0.14 cm.

Figure 7 Energy deposition density divided by various incident proton energies as function of radius at shower maximum in graphite. Beams have two sizes:
1) σ_v = 0.07 cm, σ_h = 0.14 cm; 2) σ_v = 0.7 cm, σ_h = 1.4 cm

Figure 8 Energy dependence of maximum energy deposition density in graphite for three incident proton beams:

● - σ_v = 0.07 cm, σ_h = 0.14 cm;

o - σ_v = 0.7 cm, σ_h = 1.4 cm;

▲ - σ_v = 2 cm, σ_h = 4 cm.

Figure 9 Maximum energy deposition density in graphite as a function of beam area for 0.1, 0.4, 1, 3 and 5 TeV incident protons. The beams are of the various shapes indicated only for 1 TeV case.

Figure 10. Enthalpy reserve for BeO and graphite as a function of temperature. Initial temperature T_0 = 20°C.

Figure 11 Square root of tolerable beam area for graphite (T_{max} = 2300°C) as a function of a number of protons per fast pulse for proton incident energies as indicated.

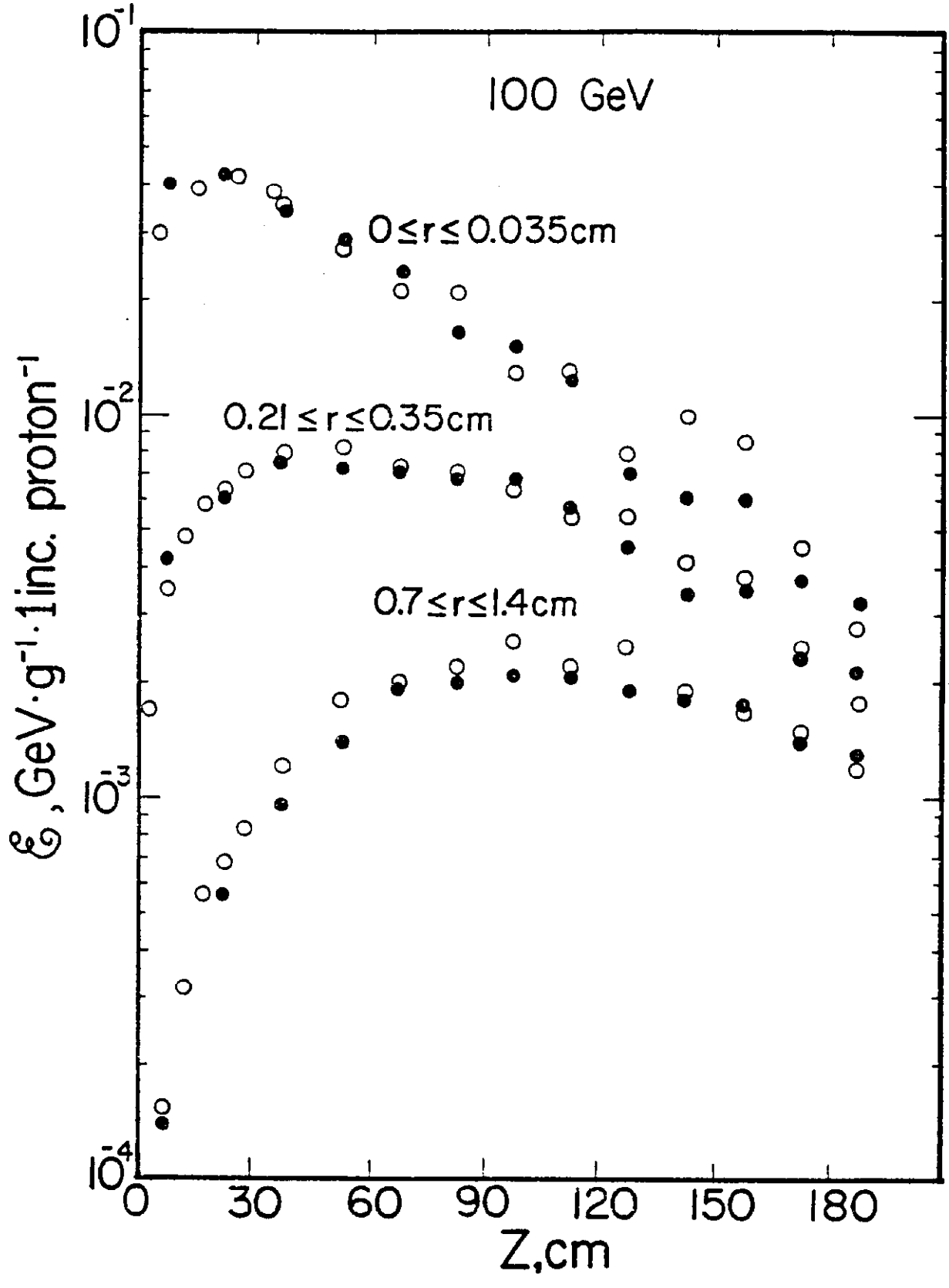
100 GeV
0≤r≤0.035cm
0.21≤r≤0.35cm
0.7≤r≤1.4cm
ε, GeV·g⁻¹·1 inc. proton⁻¹
Z, cm
10⁻¹
10⁻²
10⁻³
10⁻⁴
0
30
60
90
120
150
180

Fig. 1

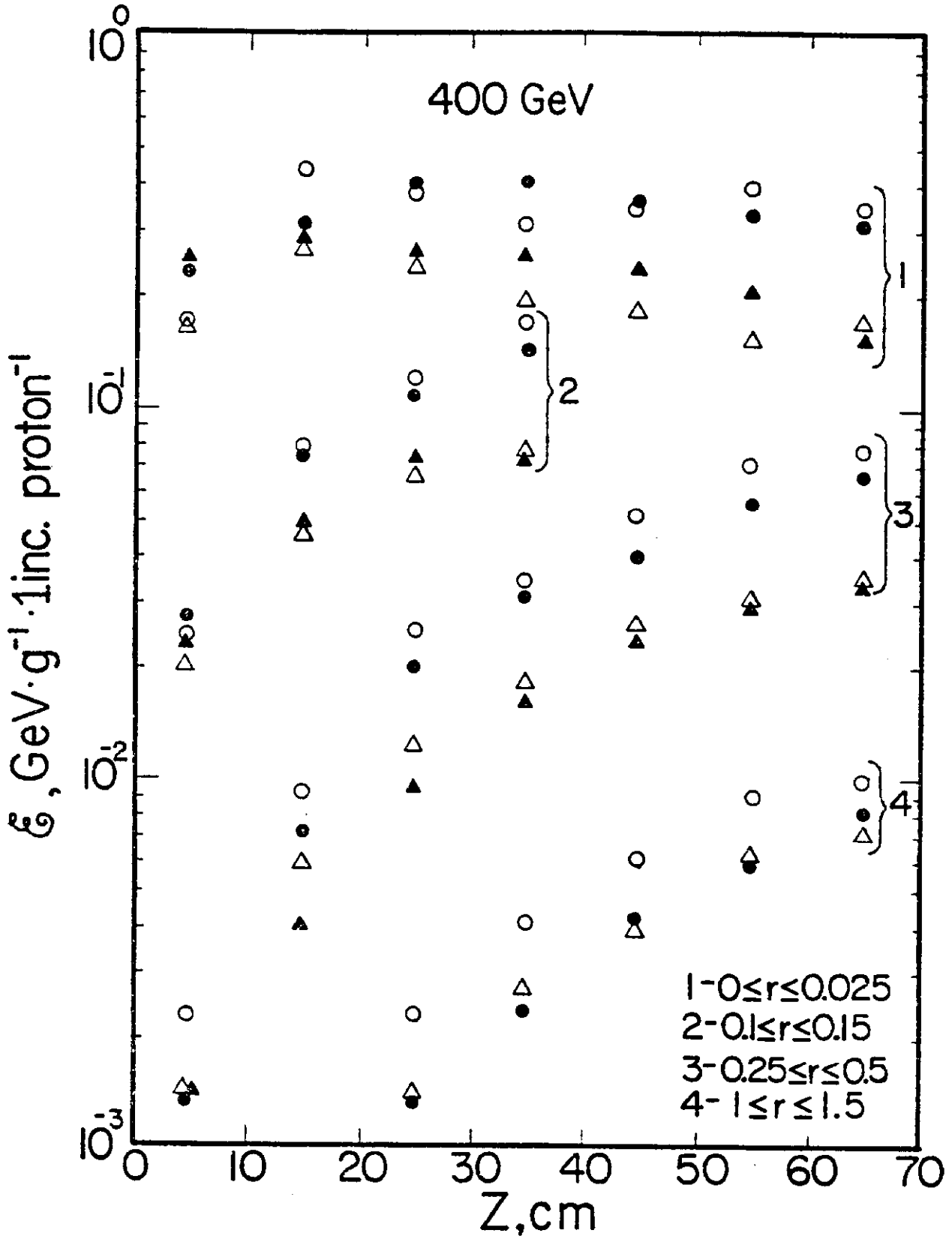
400 GeV
10^0
10^{-1}
10^{-2}
10^{-3}
$\mathcal{E}$, GeV·g^{-1}·1inc. proton^{-1}
0
10
20
30
40
50
60
70
Z,cm
1
2
3
4
1-0≤r≤0.025
2-0.1≤r≤0.15
3-0.25≤r≤0.5
4-1≤r≤1.5

Fig. 2

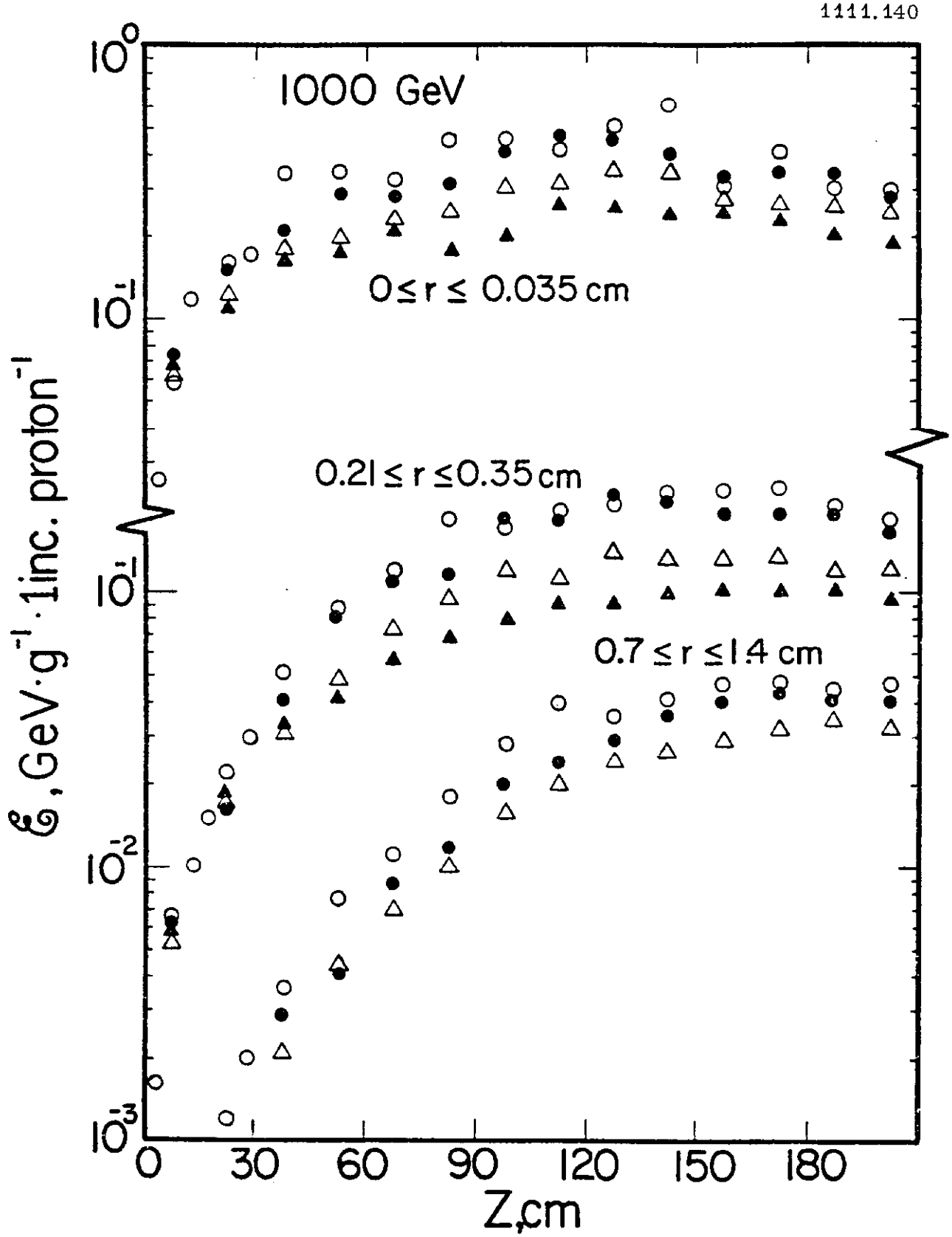
1000 GeV
0≤r≤0.035 cm
0.21≤r≤0.35 cm
0.7≤r≤1.4 cm
ε, GeV·g⁻¹·1inc. proton⁻¹
Z,cm
10⁰
10⁻¹
10⁻²
10⁻³
0
30
60
90
120
150
180

Fig. 3

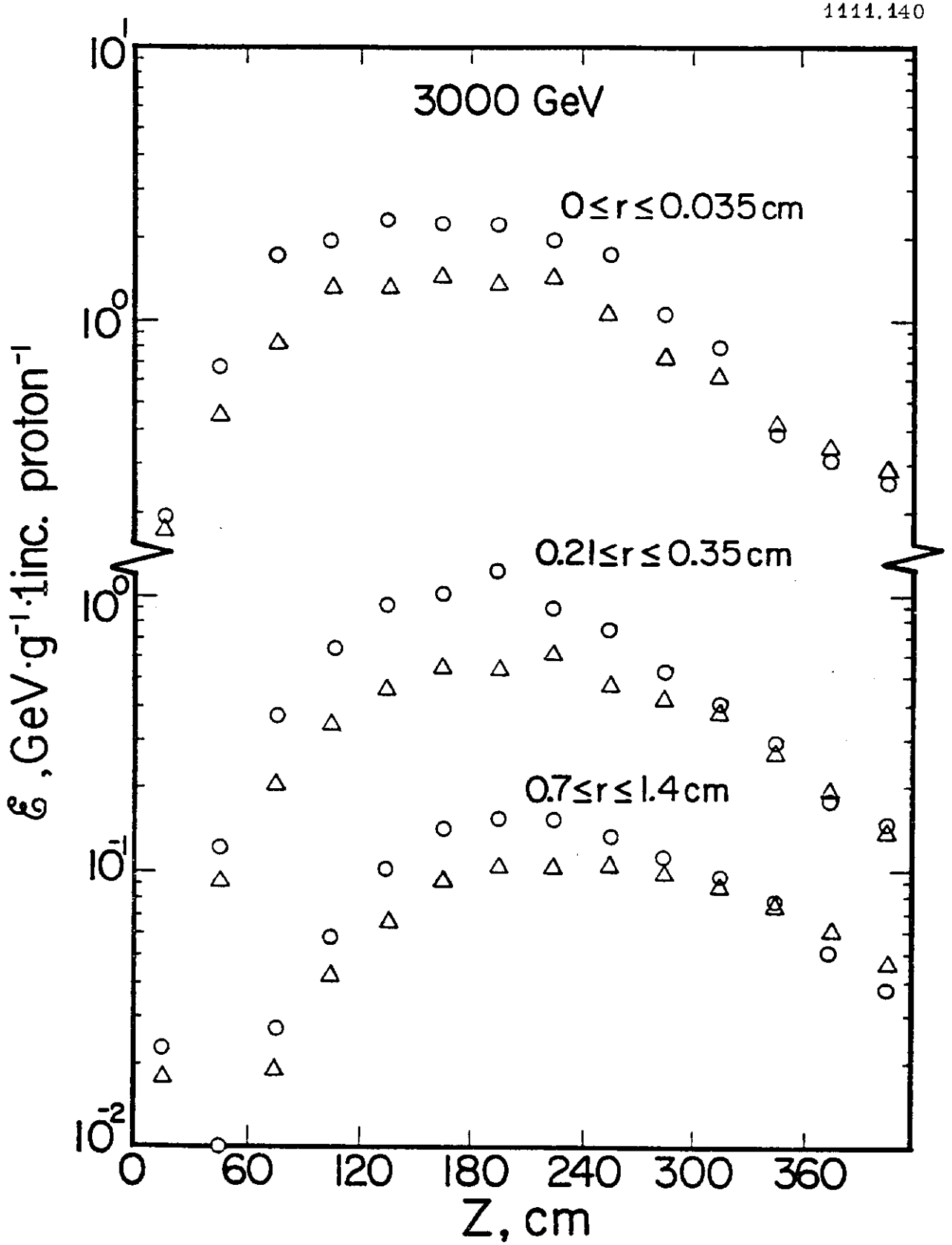
3000 GeV
0≤r≤0.035cm
0.21≤r≤0.35cm
0.7≤r≤1.4cm
ε, GeV·g⁻¹·1inc. proton⁻¹
Z, cm
10⁻¹
10⁰
10⁰
10⁻¹
10⁻²
0
60
120
180
240
300
360

Fig. 4

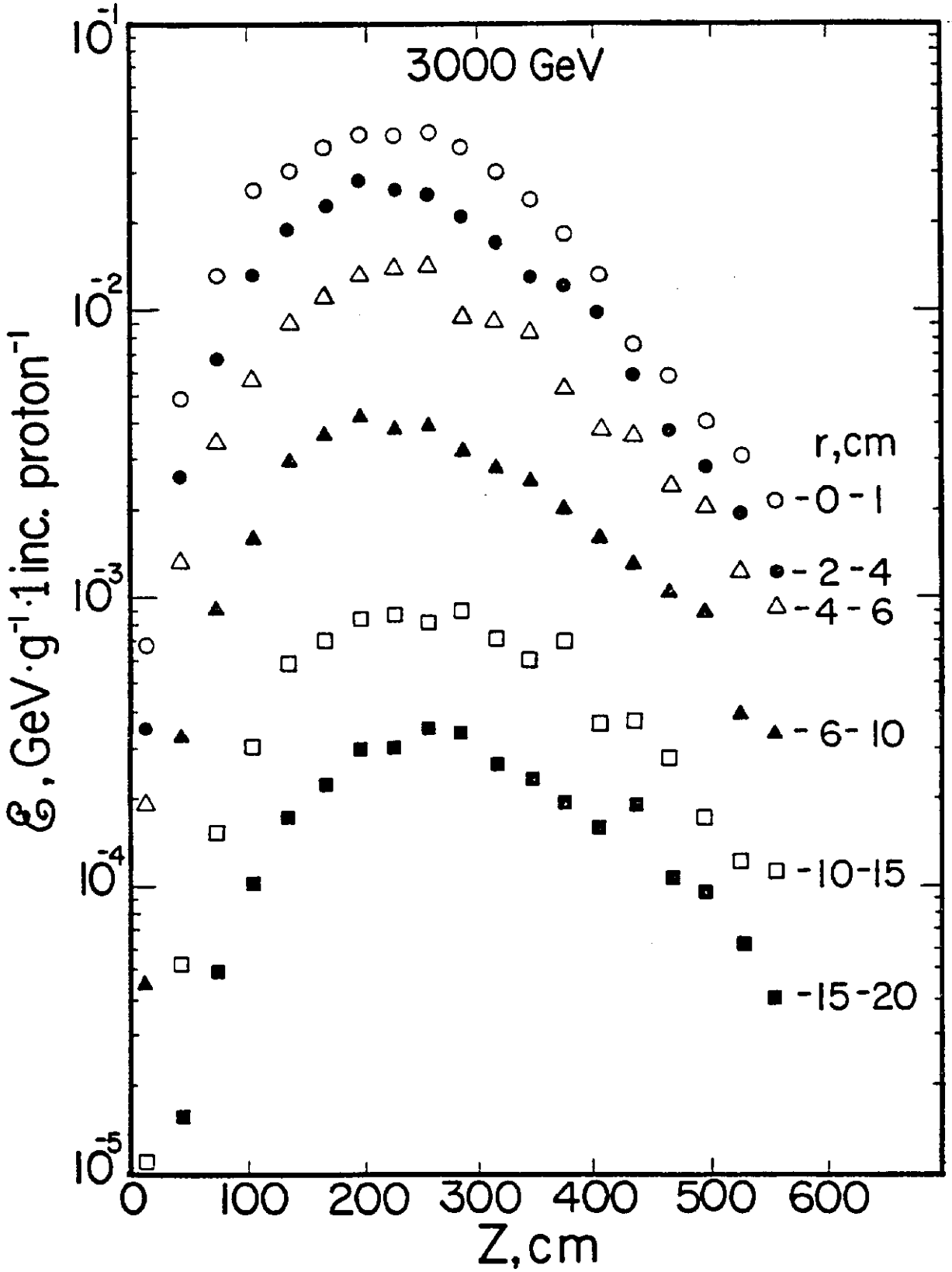
3000 GeV
10^{-1}
10^{-2}
10^{-3}
10^{-4}
10^{-5}
$\mathcal{E}$, GeV·g^{-1}·1 inc. proton^{-1}
0
100
200
300
400
500
600
Z, cm
r, cm
-0-1
-2-4
-4-6
-6-10
-10-15
-15-20

Fig. 5

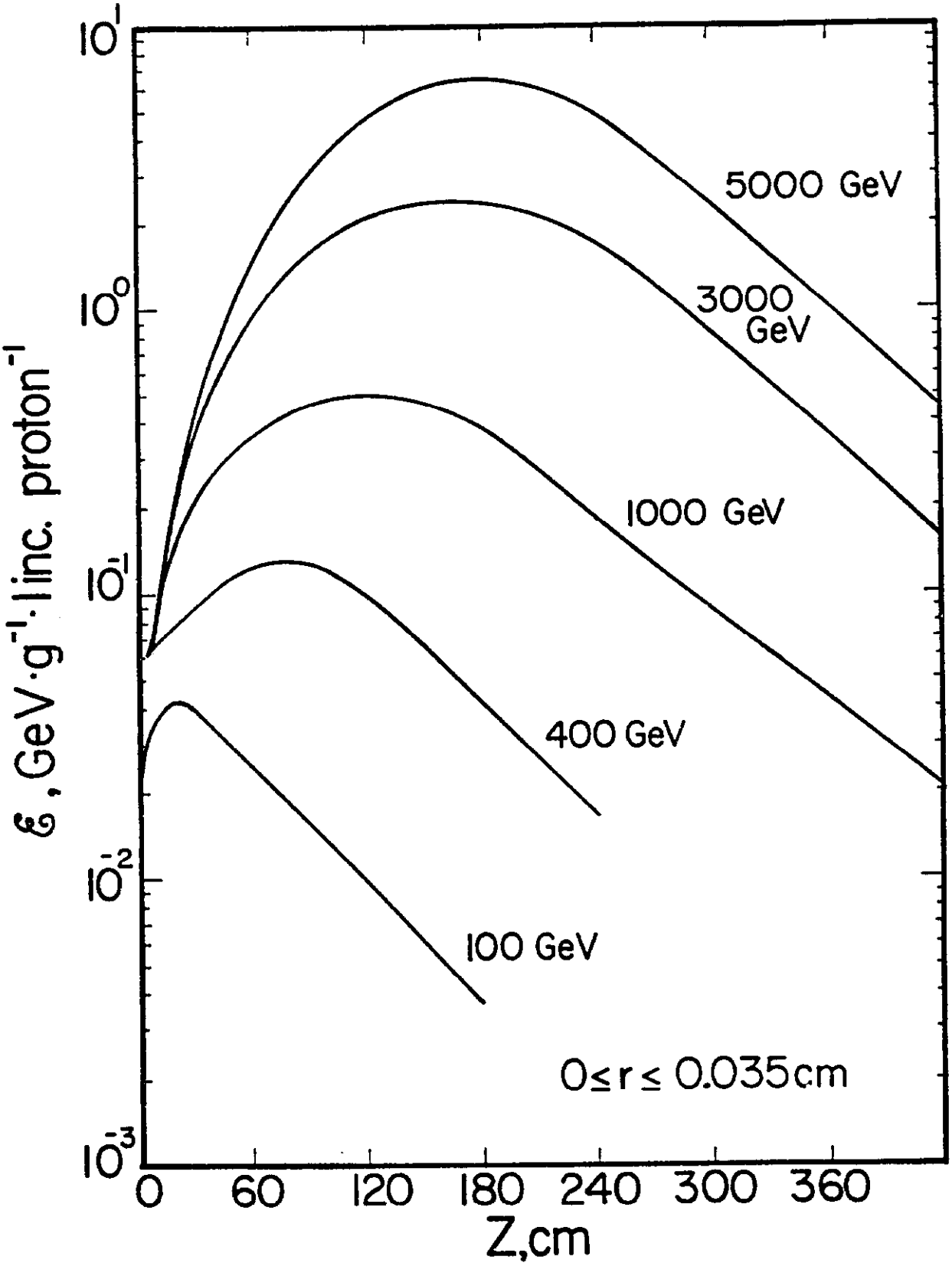
10^1
10^0
10^{-1}
10^{-2}
10^{-3}
$\mathcal{E}$, GeV·g^{-1}·1inc. proton^{-1}
5000 GeV
3000 GeV
1000 GeV
400 GeV
100 GeV
0≤r≤ 0.035cm
0
60
120
180
240
300
360
Z,cm

Fig. 6

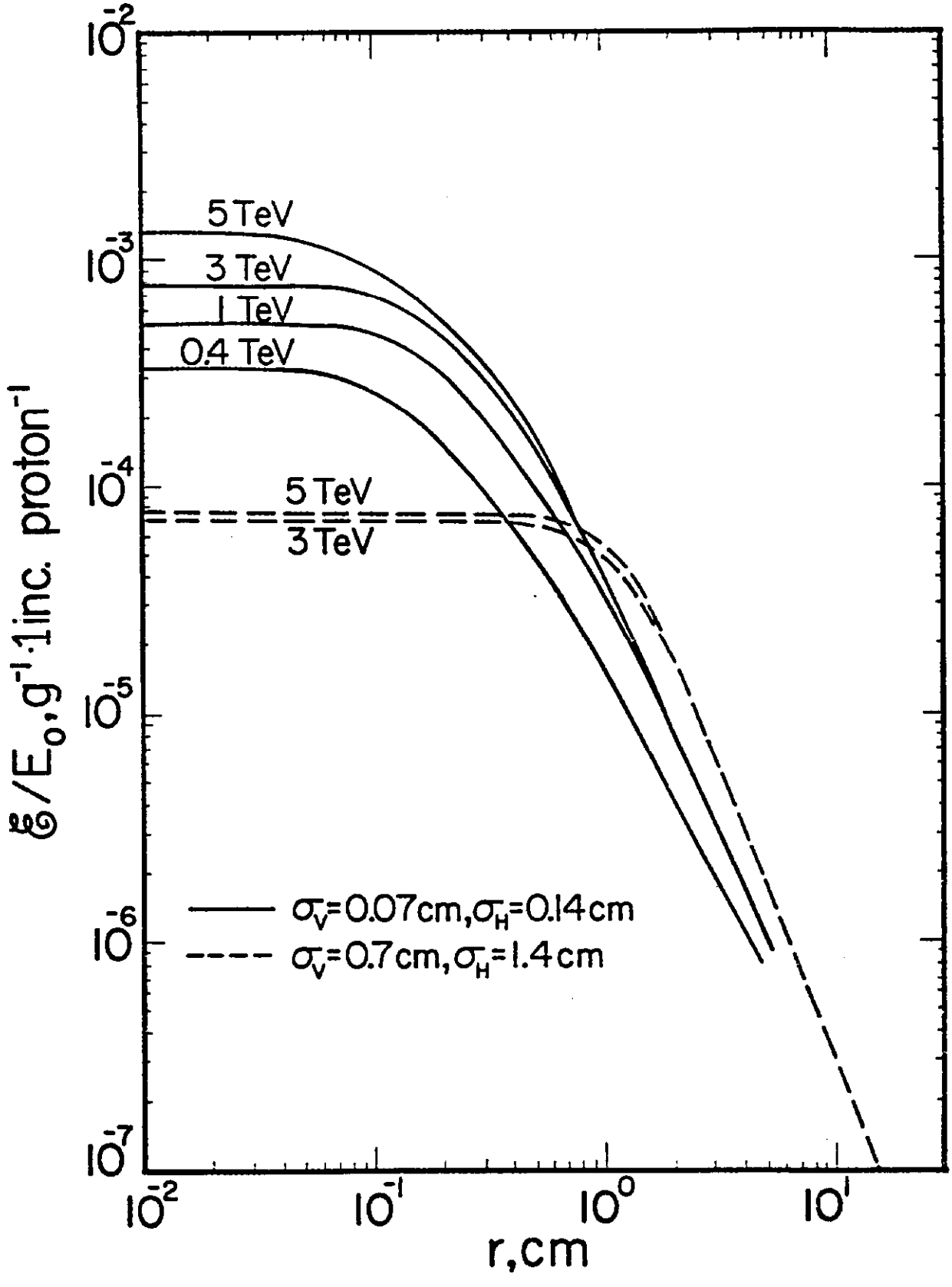
5 TeV
3 TeV
1 TeV
0.4 TeV
5 TeV
3 TeV
σ_V=0.07cm, σ_H=0.14cm
σ_V=0.7cm, σ_H=1.4cm
$\mathcal{E}/E_o$, g^{-1}·1inc. proton^{-1}
r, cm

Fig. 7

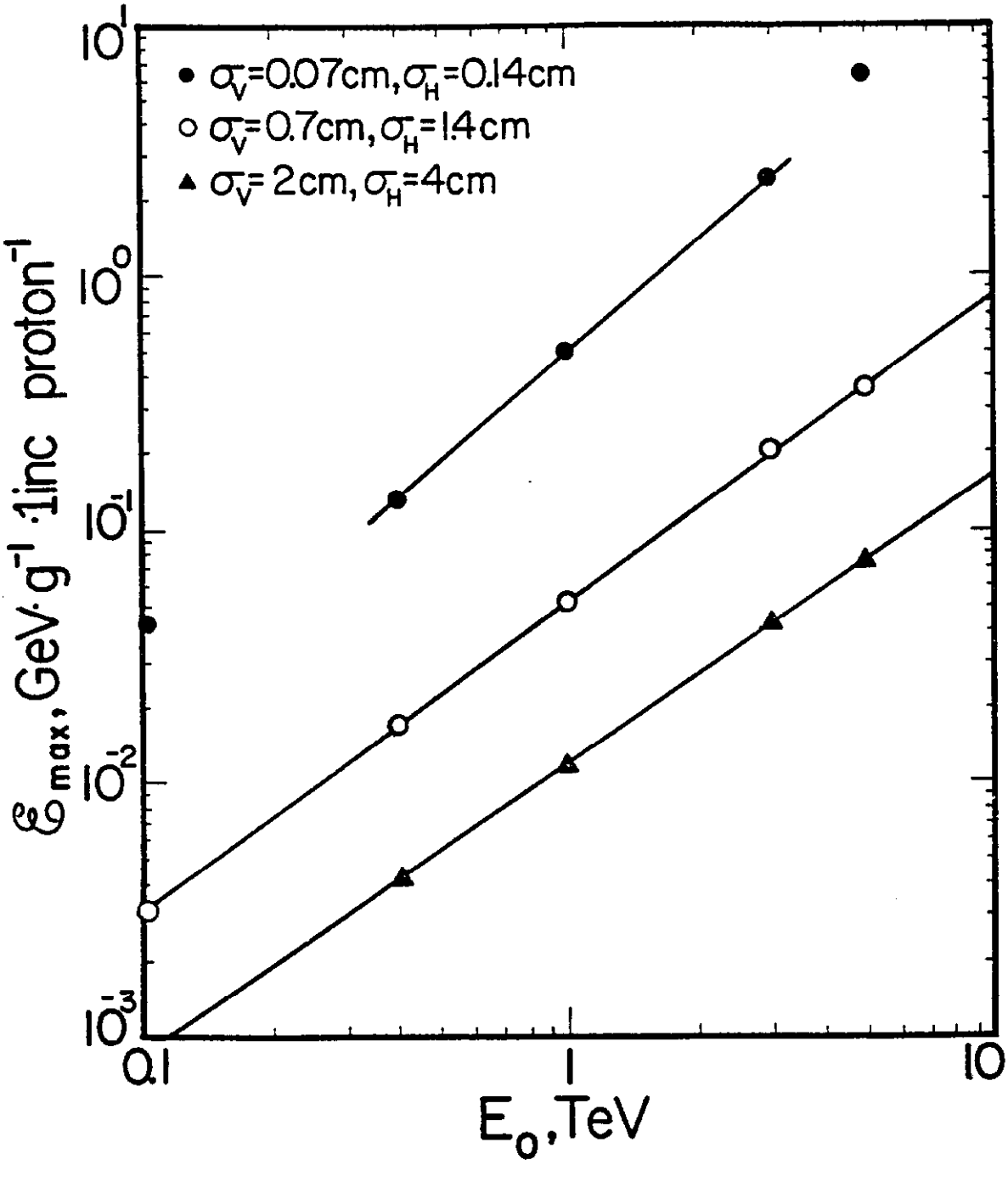
σ_V=0.07cm, σ_H=0.14cm
σ_V=0.7cm, σ_H=1.4cm
σ_V= 2cm, σ_H=4cm
$\mathcal{E}_{max}$, GeV·g^{-1}·1inc proton^{-1}
10^{1}
10^{0}
10^{-1}
10^{-2}
10^{-3}
0.1
1
10
E_0, TeV

Fig. 8

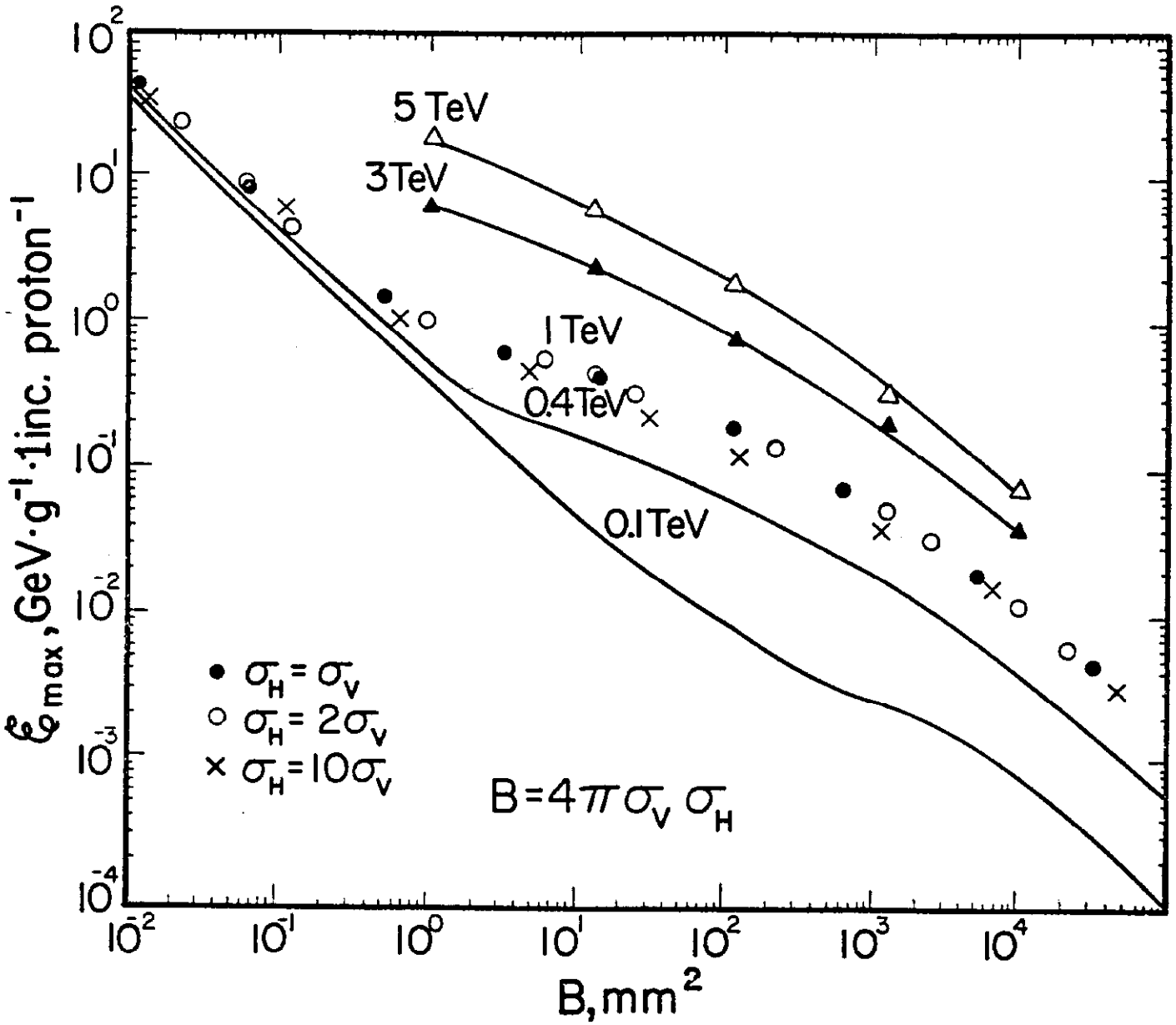
5 TeV
3TeV
1 TeV
0.4TeV
0.1TeV
$\sigma_H = \sigma_V$
$\sigma_H = 2\sigma_V$
$\sigma_H = 10\sigma_V$
$B = 4\pi\sigma_V\sigma_H$
ε_{max}, GeV·g^{-1}·1inc. proton^{-1}
B, mm^2

Fig. 9

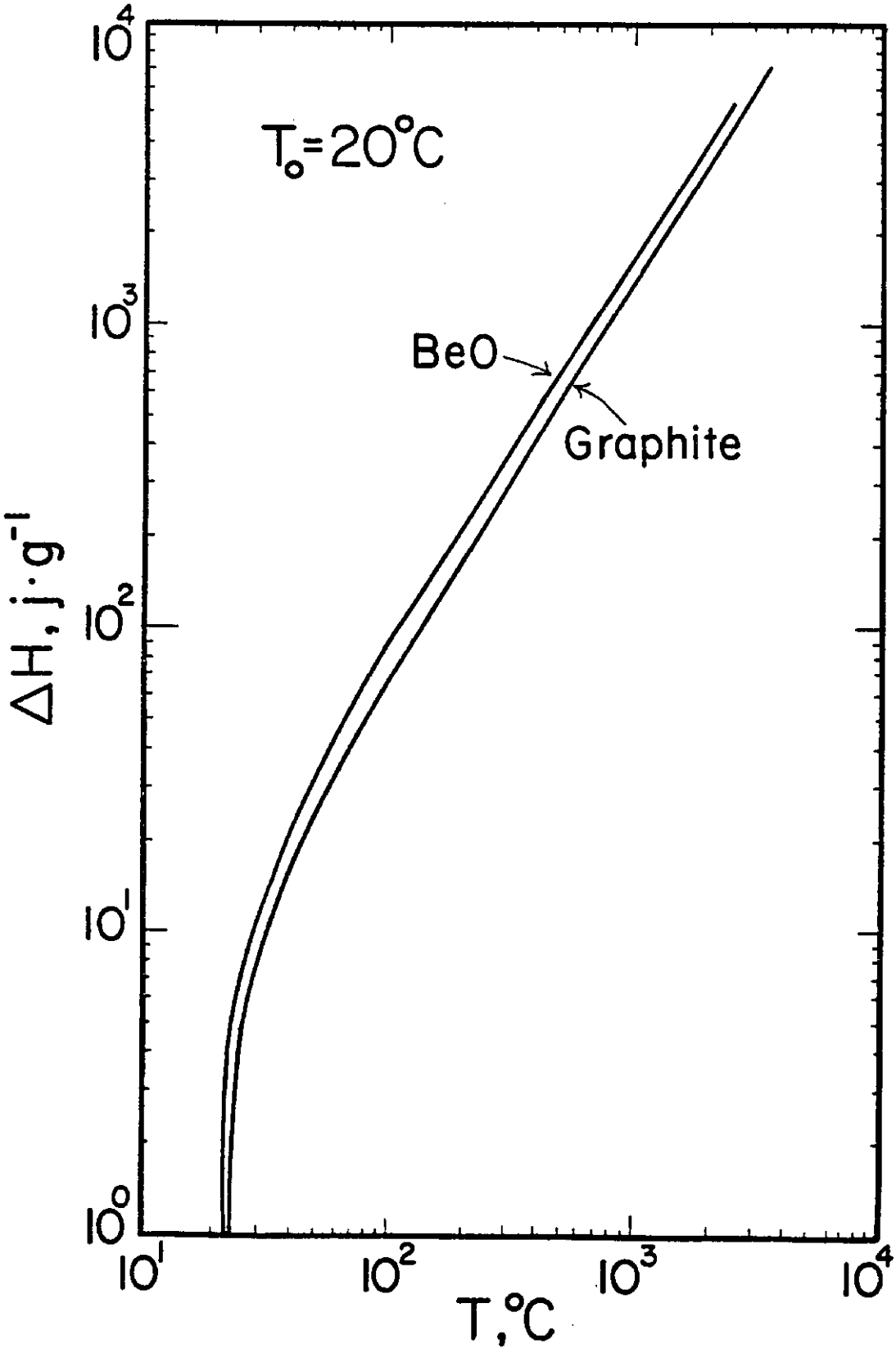
T_o=20°C
BeO
Graphite
$\Delta H, j \cdot g^{-1}$
10^4
10^3
10^2
10^1
10^0
10^1
10^2
10^3
10^4
T,°C

Fig. 10

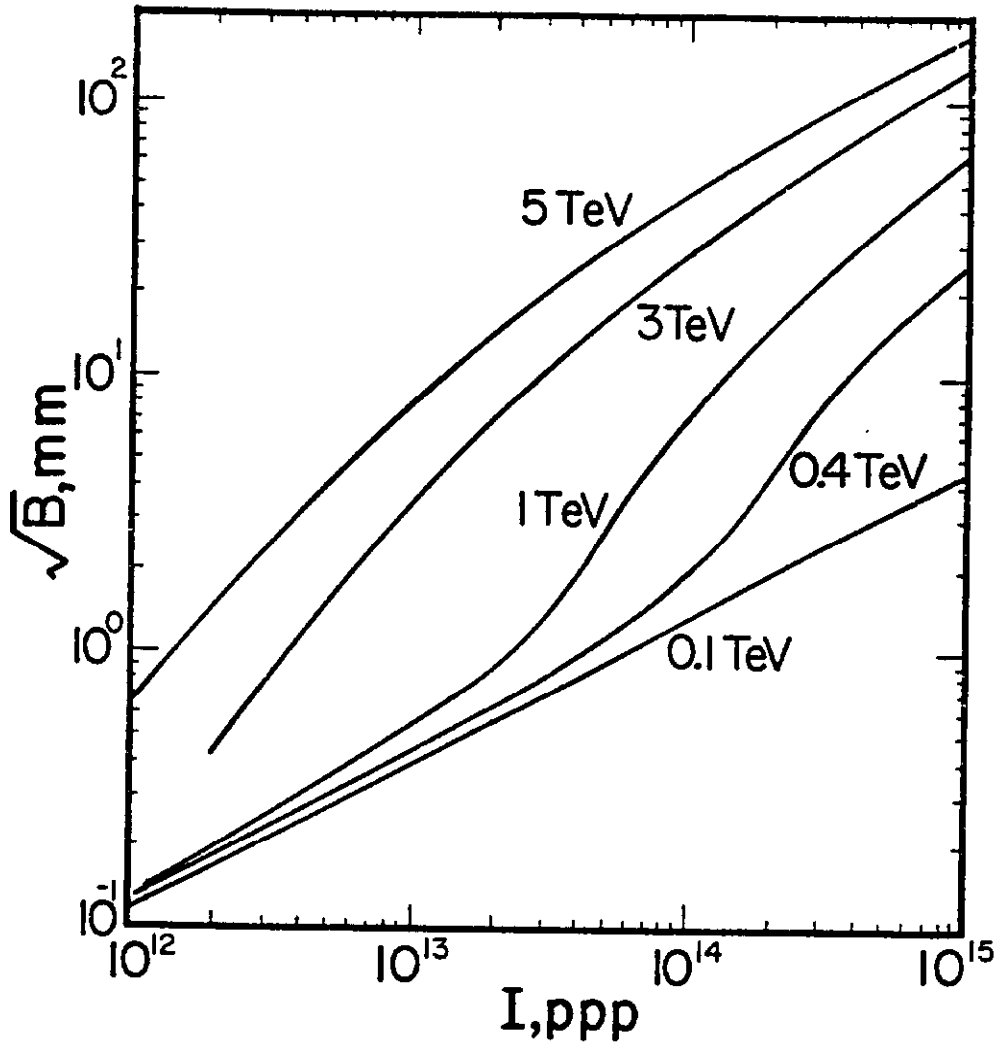
5 TeV
3 TeV
1 TeV
0.4 TeV
0.1 TeV
$\sqrt{B}$,mm
10^2
10^1
10^0
10^{-1}
10^{12}
10^{13}
10^{14}
10^{15}
I,ppp

Fig. 11